Metastable phases and phase diagrams

M. Baricco, M. Palumbo, D. Baldissin, E. Bosco, L. Battezzati

In this paper, the basic features of the novel field of the use of phase diagrams for the description of metastability will be outlined. Examples of experimental determination and calculation of metastable phase diagrams will be presented. In particular, metastable phase diagrams will be used to describe phase selection in cast iron (Fe-C) and stainless steels (Fe-Ni-Cr), showing the effect of quenching rate on solidification products. The extension of solid solubility by rapid solidification will be shown for the Au-Fe system, where giant magnetoresistance effects have been observed after suitable thermal treatments. Glass formation either by rapid solidification or by ball milling will be described in terms of metastable phase diagrams for Cu-Ti and Al-Ti. The formation of metastable compounds will be reported in Fe-B and Ni-B systems. Finally, the formation of nanocrystals from amorphous precursors will be described for Al-Ce and Al-Ni-Ce on the basis of calculated metastable phase diagrams.

Parole chiave: physical metallurgy, modelling, phase transormation, solidification

INTRODUCTION

Metastability is not a novelty in metallurgy and metallic materials are often composed by non-equilibrium phases. A well-known example is the Fe-C phase diagram, which is usually reported considering both graphite and cementite [1]. The Fe-Fe_3C equilibrium lines stand at lower temperatures with respect to Fe-C lines, indicating the metastability of the phase diagram containing cementite.

A general approach to describe stability, instability and metastability is based on energetic terms (usually Gibbs free energy). If the free energy of a system is plotted as a function of possible arrangements of atoms, the presence of maxima and minima is generally observed, as schematically shown in figure 1. The maxima correspond to unstable states, where the free energy can be easily lowered by localized homophase atomic rearrangements. The decrease of free energy drives the system towards a minimum. The absolute minimum corresponds to the stable state and, in order to transform the system, an external energy input is necessary. Relative minima correspond to metastable states, where the system is in internal equilibrium, though its free energy is above that of the stable state. There are several possible metastable conditions for a system and they are selected by kinetics. The various degree of stability can be usefully described by means of thermodynamics, whereas the description of transformations between them needs the knowledge of relative rates.

In this paper, the basic features of the novel field of the use of phase diagrams for the description of metastability will be outlined. Examples of experimental determination and calculation of metastable phase diagrams will be presented. In particular, metastable phase diagrams will be used to describe phase selection in cast iron (Fe-C) and stainless steels (Fe-Ni-Cr), showing the effect of quenching rate on solidification products. The extension of solid solubility by rapid solidification will be shown for the Au-Fe system, where giant magnetoresistance effects have been observed after suitable thermal treatments. Glass formation either by rapid solidification or by ball milling will be described in terms of metastable phase diagrams for Cu-Ti and Al-Ti. The formation of metastable compounds will be reported in Fe-B and Ni-B systems. Finally, the formation of nanocrystals from amorphous precursors will be described for Al-Ce and Al-Ni-Ce on the basis of calculated metastable phase diagrams.

Marcello Baricco, Mauro Palumbo, Daniele Baldissin, Enrica Bosco, Livio Battezzati
Dipartimento di Chimica IFM, INFM/INSTM, Università di Torino

Paper presented at the seminar: Phase transformations and phase diagrams, Milan 23 september 2003

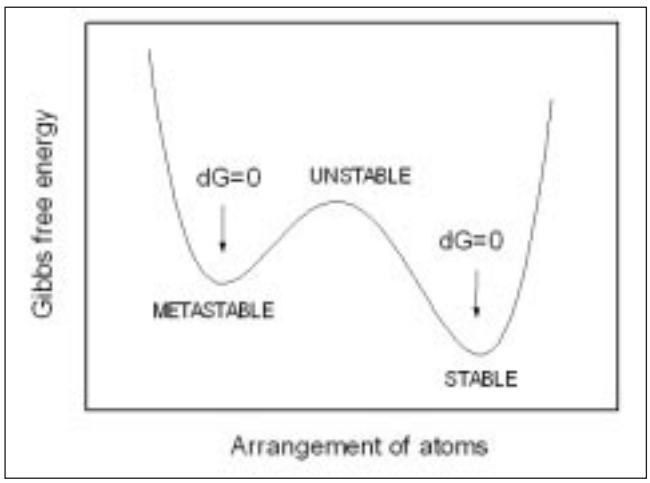

Fig. 1 – Schematic behaviour of free energy of a system as a function of possible arrangements of atoms.

Fig. 1 – Comportamento schematico dell'energia libera di un sistema in funzione della disposizione degli atomi.

METASTABILITY

The progressive departure from equilibrium to non-equilibrium conditions, through various metastable states, can be described in terms of energy units. Metastability can be classified according to structural variety and energetic departures from stable equilibrium (Table 1) [2]. The departure from the equilibrium may be scaled by means of the product RT_m, where R is the gas constant and T_m is the average of the equilibrium melting temperatures of the components. Compositional metastability involves changes in composition and implies the highest excess energy ($\approx 1\ RT_m$). Structural metastability is for phases with the same composition but a different structure and, in this case, the energy difference is about $0.5\ RT_m$. Finally, for different morphogy of the phases the excess energy is around $0.1\ RT_m$. The general procedure for the synthesis of metastable phases is to "energize" and then "quench" the material. This can be done by means of a variety of methods, as shown in Table 2 [2].

The synthesis of metastable structures can occur only when

Nature of metastability	Examples
COMPOSITIONAL	Supersaturated solutions
STRUCTURAL	Intermetallic compounds Undercooled liquid Amorphous phases
MORPHOLOGICAL AND TOPOLOGICAL	Nanocrystals Interphase dispersion

Table 1 – Nature of metastability (after reference [2]).

Tabella 1 – Natura della metastabilità (dal riferimento [2]).

Method	Examples
MELT OR SOLID QUENCH	Conventional casting Rapid solidification Laser pulse
CONDENSATION	Vapour - Gas Sputtering Electrodeposition Chemical deposition
IRRADIATION	Particle bombardment Ion implantation Ion beam mixing
MECHANICAL COLD WORKING	Ball milling Cold rolling Pressure
SOLID STATE REACTION	Multilayers

Table 2 – Methods for synthesis of metastable structure (after reference [2]).

Tabella 2 – Metodi di sintesi di strutture metastabili (dal riferimento [2]).

the kinetically preferred path differs from the one most favoured thermodynamically. It is generally the one requiring less correlation of atomic positions and motions. Whether a microstructure is composed of stable equilibrium phases or metastable phases depends on the nucleation and growth kinetics of the competing product phases. So, the thermodynamic description of metastable phases is also necessary to model the kinetics of phase transformations.

METASTABLE PHASE DIAGRAMS

Phase stability in a particular system is generally represented in terms of temperature and composition by means of the phase diagram [3] that can be drawn if the free energy of all phases is known as a function of temperature and composition. The equilibrium conditions are reached when the pure components have the same chemical potential in the different phases (common tangent rule). Metastable phase diagrams do not take into account phases, which cannot be produced for, some kinetic reasons, but consider other phases, which would not be allowed according to thermodynamics. As a consequence, in addition to the free energy of stable phases, the free energy of metastable phases has to be known. If there are kinetic reasons, which promote metastable phases, the common tangent rule is applied to the new equilibria and the phase diagram is modified accordingly becoming a metastable phase diagram. The major changes are the elimination of phases, substitution of phases, appearance of new phases, supercooling or superheating of existing phases [3].
When possible, metastable phase diagrams are determined with the same experimental techniques used for the study of equilibrium phase diagrams (i.e. thermal analysis, X-ray diffraction, TEM, SEM, etc.) but, owing to the difficulty in the experimental determination, they are often calculated. In order to obtain a metastable phase diagram, it is necessary to calculate the equilibrium phase diagram and to be able to extrapolate it to metastable conditions. In general, various models can describe accurately the equilibrium phase diagram, but extrapolations to metastable conditions may give quite different results [4]. Phase diagrams can be computed if experimental data exist for a given system. Then, a least-squares optimisation procedure gives parameters able to describe the free energy of all phases as a function of temperature and composition. This is known as CALPHAD approach [5]. The input data are the available measured thermodynamic properties and also experimentally derived portions of the phase diagram of a given system. The metastable phase diagram can be calculated simply by extrapolation of the free energy curves. This procedure is very sensitive to the analytical description of the thermodynamic functions and can give wrong results. So, more conveniently, the metastable phase diagram can be calculated if the input experimental data refer directly to metastable phases.

UNDERCOOLED MELTS AND GLASS FORMATION

In order to form a glass, a suitable melt must be undercooled to the temperature range where it freezes to an amorphous solid. For glass-forming alloys, the difference in C_p between liquid and solid phases is generally higher with respect to that of pure metals [6]. The general trend of the liquid specific heat in glass forming alloys is to increase for increasing undercooling. An higher value of the specific heat for the liquid with respect to the crystals would let the entropy of the liquid phase approach that of the solids quickly on decreasing the temperature. As the liquid cannot have an entropy lower than the solid (Kauzmann paradox), the entropy loss of the liquid on undercooling will stop when the entropy of both phases is equal (isoentropic temperature, T_K). The liquid transforms to a glass and the C_p of the liquid becomes equal to that of the solid. This is a common behaviour for glass-forming materials and the value of T_K strongly depends on the difference in specific heat between liquid and solid for temperatures lower than T_m [7]. T_K can be taken as an approximation of the glass transition temperature, T_g.

T_0 CURVES

The T_0 curve is the locus of the compositions and temperatures where the free energies of two phases are equal. The T_0 curve between the liquid and a solid phase determines the minimum undercooling of the liquid for the partition-less formation of the solid with the same composition [8]. For an estimation of the T_0 curve, the free energy of liquid and solid phases as a function of composition and temperature must be known.
Examples are provided in figure 2 for a eutectic system. T_0 curves can be confidently extrapolated at temperatures below the horizontal, where they define the temperature-composition field for partitionless solidification. Alloys with T_0 curves which are only slightly depressed below the stable liquidus curves are good candidates for partitionless solidification in the entire composition range (dashed lines in figure 2). If T_0 curves plunge to very low temperatures (thick continuous lines in figure 2), single phase crystals cannot be formed from the melt. In this region, the kinetics of solid phase separation from the undercooled liquid depresses the solidification temperature toward T_g, where an increased liquid viscosity halts crystallization, so that a glass may be formed.

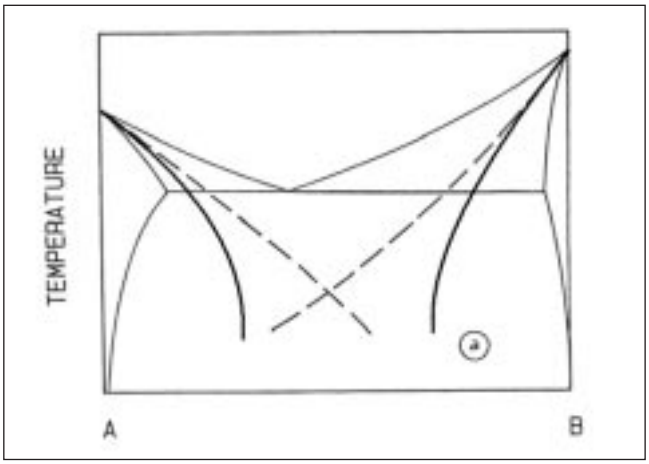

Fig. 2 – Schematic representation of T_0 curves (dashed lines) for a eutectic system. Thick continuous lines show the effect of excess specific heat of liquid phase on T_0 curves.

Fig. 2 – Rappresentazione schematica delle curve T_0 (linee tratteggiate) per un sistema eutettico. Le linee continue più spesse mostrano l'effetto del calore specifico di eccesso della fase liquida sulle curve T_0.

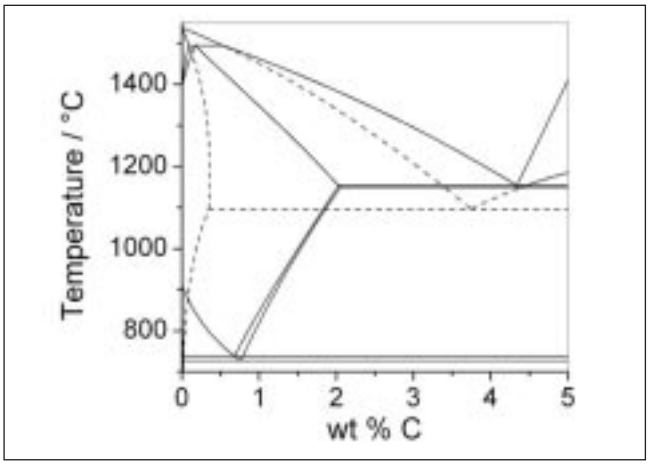

Fig. 3 – Computed stable (Fe-C) and metastable (Fe-Fe_3C) phase diagrams, continuous lines. Dashed lines give the ferrite-cementite metastable phase diagram, obtained suspending the austenite phase.

Fig. 3 – Diagrammi di fase di equilibrio (Fe-C) e metastabile (Fe-Fe_3C), linee continue. Le linee tratteggiate indicano il diagramma di fase metastabile ferrite-cementite, ottenuto sospendendo la fase austenite.

PHASE SELECTION IN CAST IRONS [9]AND STAINLESS STEELS

Rapid solidification by melt spinning was performed to check for the extent of undercooling in cast iron. All experiments were made with binary eutectic cast irons prepared by arc melting from high purity parent elements. From the analysis of phase composition and microstructure, the occurrence of the ferrite-cementite eutectic has been supposed. The binary Fe-C phase diagram has been calculated from the optimised version [10]. The results are shown in figure 3, where the austenite-graphite and austenite-cementite eutectics are easily recognised (full lines). Extending the ferrite solidus and liquidus and the cementite liquidus, i.e. suspending the austenite from the calculation, gives a metastable eutectic line at 1100 °C with the eutectic concentration at 3.8 wt% C (dashed lines). The liquid undercooling needed to produce this eutectic just exceeds 50 degrees, an amount easily obtained in rapidly solidification.

Fe-Ni-Cr is the base system for stainless steels, where the concentration of Cr must be higher than 18%. Assessed databases are available for the ternary system [11] and pseudo-binary phase diagram can be calculated. Sections of the ternary stable and metastable phase diagrams, calculated for a fixed Cr content of 18 wt%, are reported in figure 4, which refers to compositions close to the boundary between ferritic and austenitic stainless steels. Continuous lines correspond to the stable phase diagram, whereas dashed and dotted-dashed lines correspond to metastable phase diagram, obtained suspending the bcc (ferrite) and the fcc (austenite) solid solutions, respectively.

Solidification paths for stainless steel may be summarised as follow:

Mode A: $L \rightarrow L + \delta \rightarrow \delta$

Mode B: $L \rightarrow L + \delta \rightarrow L + \delta + \gamma \rightarrow \delta + \gamma$

Mode C: $L \rightarrow L + \gamma \rightarrow L + \gamma + \delta \rightarrow \gamma + \delta$

Mode D: $L \rightarrow L + \gamma \rightarrow \gamma$

where L is the liquid and δ and γ represent ferrite and austenite phases, respectively, as schematically shown on the vertical sections in the Fe-Ni-Cr phase diagram shown in figure 4. In solidification modes A and B the equilibrium primary phase is ferrite, while in modes C and D the primary phase is austenite. Solidification paths may be modified as a function of cooling rate [12]. In fact, when compositions corresponding to modes A and B are solidified at high cooling rates, some undercooling of the liquid may promote the nucleation of metastable austenite instead of stable ferrite. In addition, as a consequence of the high solidification rates, short diffusion distance are involved, leading to fine and homogeneous microstructures. Both effects appear suitable for a significant improvement of mechanical properties of the material. From the analysis of stable and metastable phase diagrams shown in figure 4, it is apparent that, in order to have a driving force for nucleation of austenite, a larger undercooling is necessary for compositions giving solidification mode A with respect to those giving solidification mode B. For instance, an alloy containing 8.5 wt% Ni (mode A) must be undercooled of about 20 K, in order to reach the metastable liquidus curve for the austenite, whereas for an alloy containing 11 wt% Ni (mode B) an undercooling of

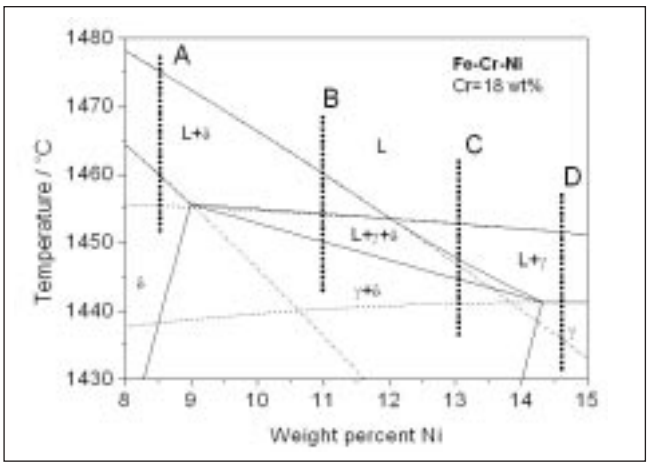

Fig. 4 – Calculated section of Fe-Ni-Cr phase diagram with 18 wt% Cr. Continuous lines: stable phase diagram; dashed lines: metastable phase diagram obtained suspending the bcc (ferrite) solid solution; dotted-dashed lines: metastable phase diagram obtained suspending the fcc (austenite) solid solution.

Fig. 4 – Sezione calcolata del diagramma di fase Fe-Ni-Cr con il 18 wt % Cr. Linee continue: diagramma di equilibrio; linee tratteggiate: diagramma metastabile ottenuto sospendendo la soluzione solida bcc (ferrite); linee tratteggiate-punteggiate: diagramma metastabile ottenuto sospendendo la soluzione solida fcc (austenite).

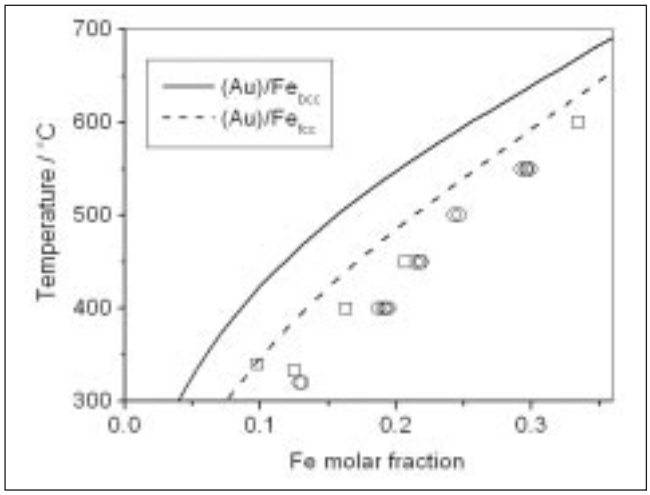

Fig. 5 – Calculated Au-Fe phase diagram: stable (Au)/Fe_{bcc} solvus (solid line) and metastable (Au)/Fe_{fcc} solvus (dashed line). Experimental data from annealing of rapidly solidified $Au_{70}Fe_{30}$ alloy (circles) and from literature (squares).

Fig. 5 - Diagramma di fase Au-Fe calcolato: solvus (Au)/Fe_{bcc} di equilibrio (linea continua) e solvus (Au)/Fe_{fcc} metastabile (linea punteggiata). I dati sperimentali si riferiscono a campioni di una lega $Au_{70}Fe_{30}$ ottenuta per rapida solidificazione e successivamente trattata termicamente a diverse temperature (cerchi) e a dati ottenuti dalla letteratura (quadrati).

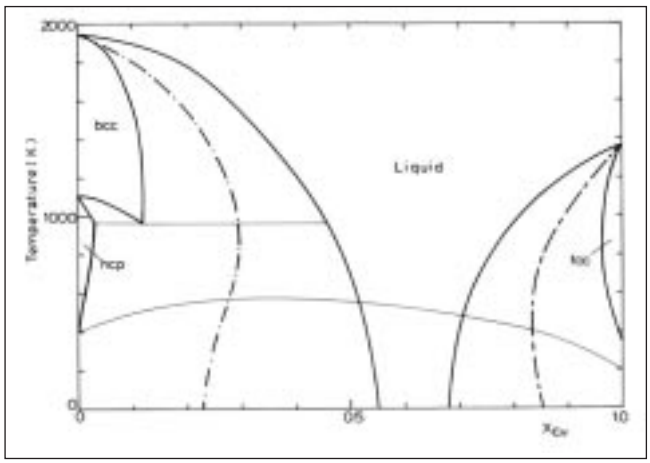

Fig. 6 – Calculated metastable Ti-Cu phase diagram and T_0 curves for bcc (dash-dotted lines) and fcc (dashed lines) solid solutions. Thin continuous line represents T_K.

Fig. 6 – Diagramma metastabile Ti-Cu (linee continue) e curve T_0 calcolate per le soluzioni solide bcc (linee tratteggiate-punteggiate) e fcc (linee tratteggiate). La linea continua sottile rappresenta la temperatura di transizione vetrosa, T_K.

about 5 K is sufficient. Rapid solidification of steels with higher Ni content (mode C) allows the formation of ferrite in undercooling conditions, so that austenite is produced from solid state transformation, reducing volume contraction and surface cracks formation [12]. A further increase of Ni content in the steel gives solidification mode D, so that austenite is formed directly from the melt with a primary reaction.

EXTENDED SOLID SOLUTIONS IN Au-Fe [13]

An interesting magnetic property, known as giant magnetoresistance (GMR), can occur when homogeneous nanosized particles of a ferromagnetic metal (for instance Fe and Co) are embedded in a paramagnetic matrix (for instance Cu and Au). This microstructure can be obtained with suitable thermal treatments of a supersaturated solid solution obtained by rapid solidification. Good candidates for such behaviour are systems partially immiscible in the solid state, which are forced into solid solution by rapid solidification. Supersaturated solid solutions have been prepared by rapid solidification in the Au-Fe system [13]. X-ray diffraction analysis showed that rapidly solidified $Au_{70}Fe_{30}$ consists of a single supersaturated solid solution of Fe in Au. In fact, a small liquid undercooling suffices to reach the T0 curve, where the liquid phase is partition-less transformed into a solid solution. After annealing in the temperature range between 320 °C and 500 °C, X-ray diffraction peaks showed significant broadening due to the simultaneous effect of crystallite size and lattice strain. In addition, peaks are shifted to lower angles on account of the increased lattice parameter of the supersaturated solid solution. The results suggest the occurrence of a discontinuous precipitation reaction of a Fe-rich fcc phase, which leaves an Au-enriched residual matrix. The composition of solid solutions obtained by XRD analysis of samples annealed until precipitation occurred at various temperatures are reported on the phase diagram shown in figure 5, together with stable bcc and metastable fcc solvus lines calculated from recent CALPHAD assessment [14]. After precipitation, compositions of the residual matrix are below the stable solvus line, which refers to the precipitation of a bcc Fe-rich phase, but are closer to the metastable solvus line calculated considering the formation of a Fe-rich fcc phase, in agreement with experimental findings.

METALLIC GLASSES IN Cu-Ti [15]AND Al-Ti [16]

The Cu-Ti phase diagram is characterized by several deep eutectics, so it is expected glass formation is feasible in a wide composition range [17]. The liquid shows a substantial degree of order, as put in evidence by experimental values of its excess specific heat [15]. The ordering effect in liquid alloys is generally composition dependent and the thermodynamic evidence of ordering is in agreement with direct structural data [18]. The C_p contribution to the free energy of the liquid in undercooling conditions becomes negligible at the ideal glass transition, T_K, where the entropy of fusion of the alloy is nil [19].
From the assessed thermodynamic parameters [17], the free energy of liquid and crystal phases has been obtained. Including the estimated values for the excess specific heat and neglecting the formation of intermetallic phases, a metastable phase diagram has been calculated (figure 6). From the calculated metastable phase diagram the amorphizing range limited by T_0 curves has been predicted, close to the experimental results.
Amorphisation in Al-Ti is not possible by rapid solidification, but it can be achieved by direct synthesis via mechanical alloying suitable blends of the elements [16]. In order to explain this result, free energy curves have been calculated at different temperatures according to the assessment reported in ref. [20]. T_0 curves have been calculated for bcc, fcc and hcp solid solutions and the results are shown in figure 7 (a), together with the equilibrium phase diagram. The curves extend in a wide composition range at high temperatures, showing that partition-less crystallisation of the liquid into solid solutions cannot be prevented during melt quenching. Since no experimental data are available for Al-Ti, an excess specific heat of the same order as for Cu-Ti has been considered to calculate free energy curves. It was shown that the temperature dependence of the thermodynamic properties of the liquid leads to an inversion of stability of the phases at low temperature. The free energy of the liquid becomes lower than that of the solid solutions and a glass forming range is predicted. In fact, considering the excess specific

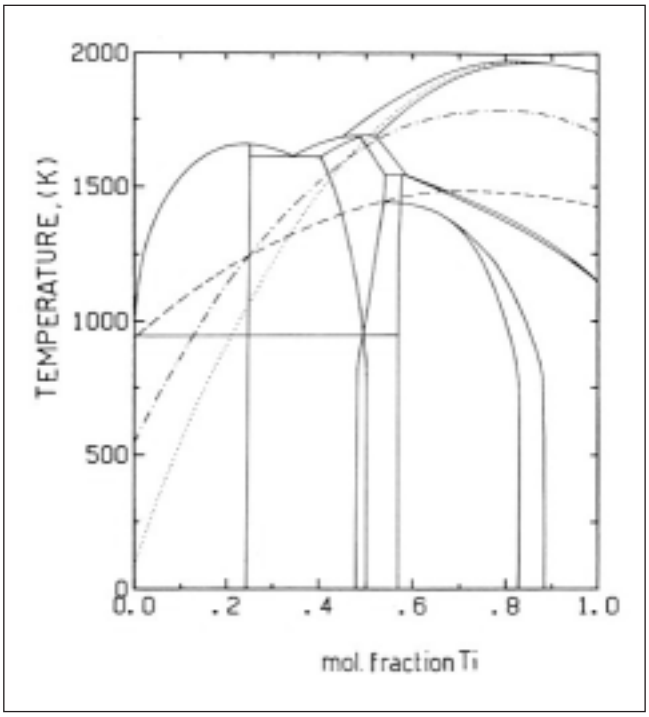

Fig. 7 (a) – Schematic Al-Ti phase diagram, with superimposed T_0 curves (after ref. [20]): dashed lines, fcc solid solution; dotted lines, bcc solid solution; dash-dotted lines, hcp solid solution.

Fig. 7 (a) – Diagramma di fase schematico Al-Ti, con le curve T_0 sovrapposte (da ref. [20]): linee tratteggiate, soluzione solida fcc; linee punteggiate, soluzione solida bcc; linee tratteggiate-punteggiate, soluzione solida hcp.

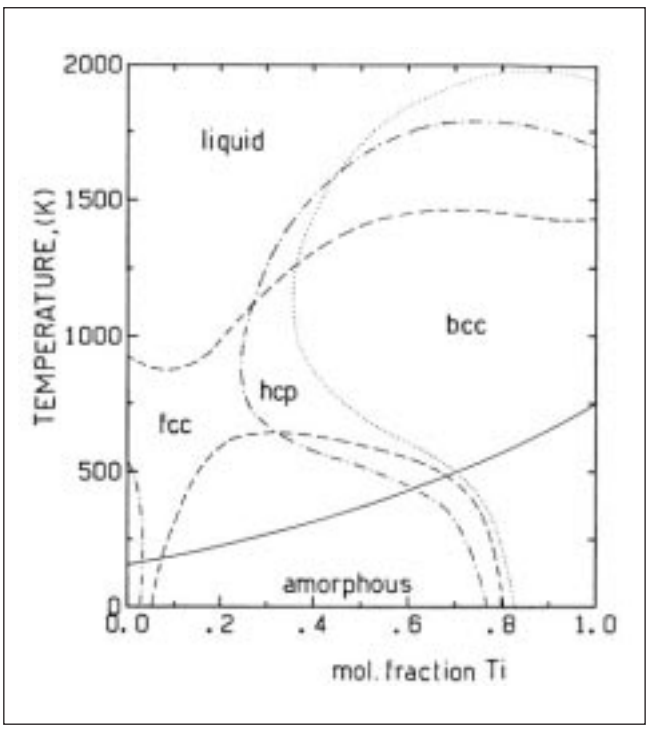

Fig. 7 (b) – T_0 curves calculated considering an excess specific heat for the liquid phase: dashed lines, fcc solid solution; dotted lines, bcc solid solution; dash-dotted lines, hcp solid solution. Continuous line gives the estimated T_K.

Fig. 7 (b) – Curve T_0 calcolate considerando un termine di calore specifico di eccesso nella fase liquida: linee tratteggiate, soluzione solida fcc; linee punteggiate, soluzione solida bcc; linee tratteggiate-punteggiate, soluzione solida hcp. La linea continua è la temperatura T_K stimata.

heat for the liquid phase, T_0 curves have been again calculated for bcc, fcc and hcp solid solutions and the results are shown in figure 7 (b). The T_0 curves still extend over wide composition ranges at high temperature but they divide up and bend at intermediate temperature, sharply restricting the range of existence of the solid solutions and opening up a glass forming range by solid state reaction.

METASTABLE COMPOUNDS IN Fe-B [21, 22, 23] AND Ni-B [21]

The Fe-B system shows a significant glass forming ability (GFA) for compositions close to the Fe-rich eutectic [24]. In order to calculate driving forces for crystallisation, a thermodynamic analysis of the system by means of the CALPHAD approach has been carried out, including metastable and amorphous phases. The set of experimental data for stable equilibria have been taken from a recent assessment, where only stable phases have been considered [25]. The metastable Fe_3B compound has been reported as a crystallisation product of amorphous alloys in the composition range between 12 and 25 at % B [26]. It decomposes to stable bcc-Fe and Fe_2B after heating at high temperatures, as confirmed by recent calorimetric investigations [21]. A eutectic temperature of 1387 K has been measured for the metastable equilibrium liquid → Fe_3B + fcc-Fe. An excess specific heat term has been added to describe the Gibbs free energy of the liquid phase on undercooling and a recent description of pure Fe lattice stabilities [27] has been used for the optimisation. The calculated equilibrium phase diagram is reported in figure 8 (full line). The agreement with experimental data is good and results related to stable phases are comparable to those obtained in previous assessments [25]. Figure 8 (dashed lines) shows also the calculated metastable phase diagram, obtained removing from the calculation the Fe_2B boride. Fe_3B becomes stable and the expected eutectic occurs at 1387 K and 18 at %B.
Various Ni-B compositions around the Ni-Ni_3B eutectic and the Ni_2B compound have been analyzed for undercooling by embedding them in a solid flux of alumina in the cell of a high temperature calorimeter [28]. This has allowed the measurement of transformation enthalpies (fusion, solidification), as a function of temperature and the estimate of the liquid specific heat in the undercooling regime. In all cases undercooling of primary, eutectic and polymorphic reactions

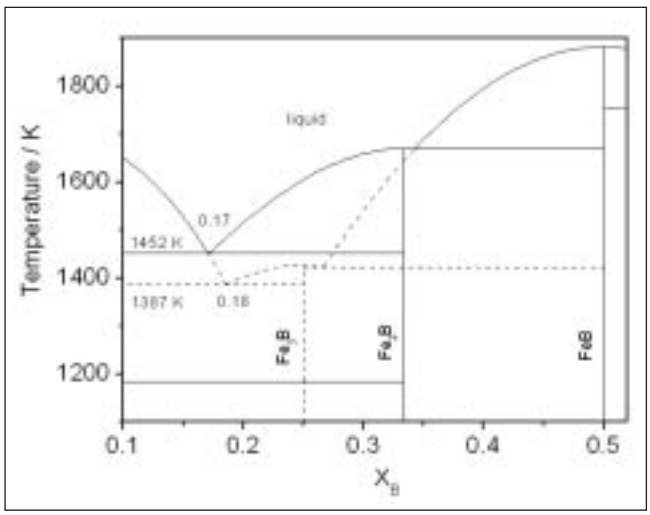

Fig. 8 – Calculated Fe-B stable (continuous line) and metastable (dashed line) phase diagrams.

Fig. 8 – Diagrammi di fase Fe-B calcolati di equilibrio (linea continua) e metastabile (linea tratteggiata).

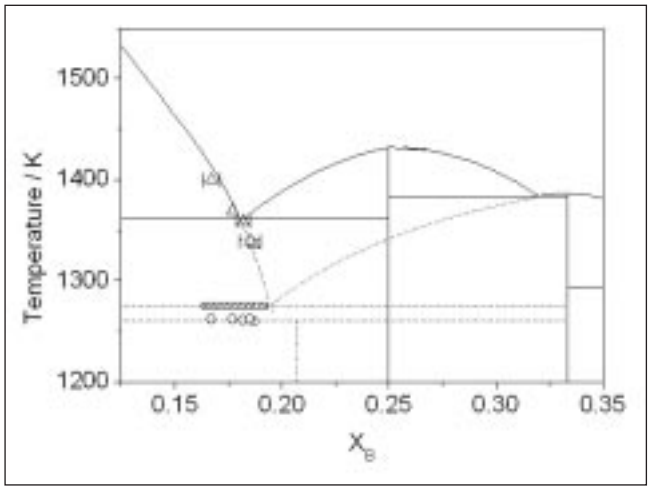

Fig 9 – Ni-B phase diagrams. Experimental points (circles giving the peritectoidic temperature and triangles giving the liquidus temperature) have been obtained from DSC analysis. Full lines: equilibrium phase diagram from literature; dashed lines: estimated metastable phase diagram.

Fig. 9 – Diagrammi di fase Ni-B. I punti sperimentali (i cerchi rappresentano la temperatura peritettoidica e i triangoli la temperatura di liquidus) sono stati ottenuti dall'analisi DSC. Linee continue: diagramma di fase di equilibrio dalla letteratura; linee tratteggiate: diagramma di fase metastabile stimato.

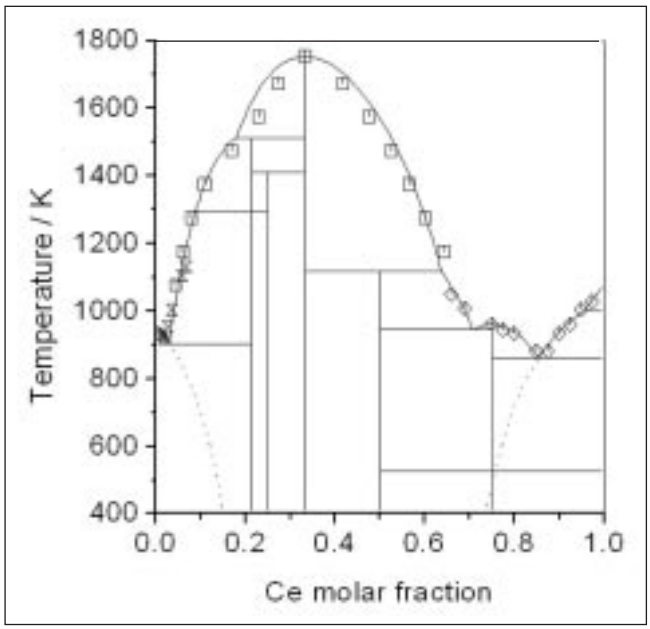

Fig. 10 – Calculated Al-Ce equilibrium (full lines) and metastable (dashed lines) phase diagram. The symbols represent experimental input data.

Fig. 10 – Diagramma di fase Al-Ce calcolato (linee continue) e metastabile (linee tratteggiate). I simboli rappresentano i dati sperimentali forniti in input.

has been obtained from a few degrees up to about 150 K. The degree of undercooling (ΔT) depends strongly on the occurrence of heterogeneous nucleation events in each experiment, so there is no correlation between ΔT and cooling rate, sample mass or alloy composition. On solidification in undercooling, a new metastable phase ($Ni_{23}B_6$) was produced. The thermal analysis curves of samples of various compositions provided a metastable Ni-B phase diagram (figure 9). The stable phase diagram, obtained from a recent CALPHAD assessment [29], is also reported for comparison. Dashed lines in figure 9 represent the calculated meta-

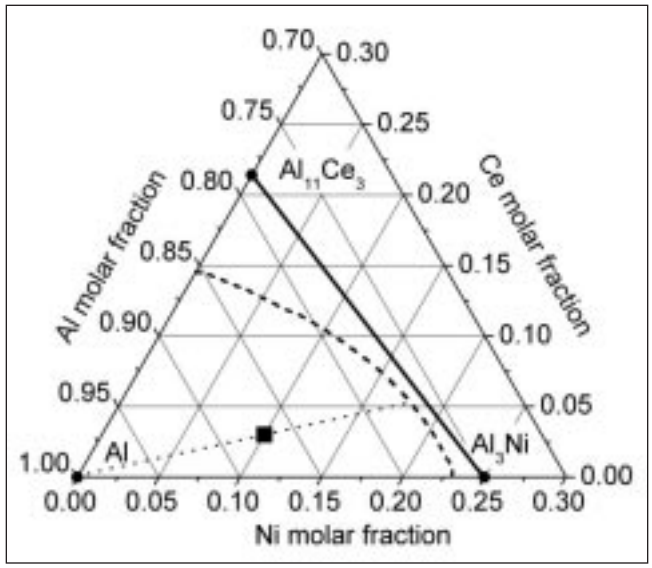

Fig. 11 – Section of metastable Al-Ni-Ce phase diagram calculated at 450 K, including fcc-Al and liquid (amorphous) phases. Dotted line gives an example of a tie-line connecting Al and residual amorphous phase in metastable equilibrium after primary crystallisation in an $Al_{87}Ni_{10}Ce_3$ amorphous alloy (square).

Fig. 11 - Sezione del diagramma di fase metastabile Al-Ni-Ce calcolata a 450 K includendo le fasi fcc-Al e liquida (amorfa). La linea punteggiata fornisce un esempio di equilibrio tra la fase alluminio e la fase amorfa residua in equilibrio metastabile dopo la cristallizzazione primaria in una lega amorfa $Al_{87}Ni_{10}Ce_3$ (quadrato).

stable Ni-B phase diagram, obtained including the $Ni_{23}B_6$ phase and suspending the Ni_3B compound. The metastable $Ni_{23}B_6$ phase decomposes on heating with a peritectoid reaction into Ni and a phase richer in B, possibly Ni_2B. The eutectic between these phases occurs a few degrees above the first transformation. From the trend of the liquidus, the metastable eutectic between Ni and Ni_2B can be located approximately at 20 at% B.

NANOCRYSTALLINE ALLOYS IN Al-Ce [30] AND Al-Ni-Ce [31]

Improved mechanical properties have been recently evidenced in different Al-RE and Al-Ni-RE (RE=rare earth) alloy systems when a nano-scale microstructure is obtained [32]. Such a microstructure may be obtained by suitable annealing of amorphous alloys. In order to illustrate the thermodynamic and kinetic aspects which promote the formation of nanocrystals by primary crystallisation in amorphous alloys, a thermodynamic assessment of stable and metastable phases has been carried out for Al-Ce and Al-Ni-Ce systems.

A thermodynamic assessments of the Al-Ce system using experimental data of stable and metastable phases has been carried out and, on the basis of the Gibbs energies obtained for all phases, the driving forces for nucleation has been calculated as a function of temperature and composition [30]. Heats of crystallization of the amorphous phase and experimentally obtained specific heats of the liquid were used for the description of the metastable states [33]. The assessed Al-Ce phase diagrams is shown in figure 10. The liquidus points are generally well reproduced and the eutectic composition was calculated at 97 Al at%. Assuming that the formation of the intermetallic compounds can be kinetically by-passed, a metastable phase diagram between the solid so-

lution of the components and the liquid or the amorphous phase has been calculated. The metastable phase diagrams predict a wide composition range of glass-formation, as shown by dashed lines in figures 10.
Thermodynamic assessments of stable binary Al-Ni [34] and Al-Ce [30,35] systems are available in the literature. In order to obtain an estimate of the thermodynamic behaviour of the Al-Ni-Ce ternary system, a new assessment of the Ni-Ce binary system has been carried out [36]. In order to simulate the primary crystallisation of fcc-Al from the amorphous phase, an estimate of the free energy of the liquid alloys has been obtained from a Muggianu's interpolation [5] of thermodynamic parameters of the binary systems. Thermodynamic properties of the solid phases have been taken from the assessed binary phase diagrams. The stable and metastable phase diagrams calculated at 450 K are shown in figure 11. The full line gives the equilibrium between stable solid phases, namely fcc-Al, Al_3Ni and $Al_{11}Ce_3$, and the dashed line gives the composition of the liquid (amorphous) phase in metastable equilibrium with Al nanocrystals. As an example, considering an $Al_{87}Ni_{10}Ce_3$ amorphous alloys, using the tie line (dotted line in figure 11) it is possible to estimate the composition of the residual amorphous matrix obtained after primary crystallisation. From the free energy values of the solid and liquid (amorphous) phases, the driving force for nucleation of Al has been calculated as a function of temperature and composition, allowing a description of nanocrystalline phase formation.

ACKNOWLEDGMENTS

This paper is a collection of results obtained in last years at the Laboratory of Metallurgy of University of Torino. The authors wish to thank prof. Carlo Antonione and prof. Gabriele Cacciamani for advises and suggestions. Work performed for PRIN 2002038584_004, PRIN 200303875_003 and MRTN-CT-2003-504692.

REFERENCES

[1] O.Kubachewski, "Iron Binary Phase Diagrams", Springer Verlag (Düsseldorf), 1982, p. 23

[2] D.Turnbull, Metall. Trans. 12B (1981) 217

[3] T.B.Massalski, Metall. Trans. 20B (1989) 445

[4] R.B.Schwarz, P.Nash, D.Turnbull, J. Mat. Res. 2 (1987) 456

[5] N.Saunders, A.P.Miodownik, "CALPHAD: a comprehensive guide", New York, Elsevier Science, 1998

[6] H.J.Fecht, Mat. Sci. Eng. A178 (1994) 61

[7] L.Battezzati, M.Baricco, Phil. Mag. B56 (1987) 139

[8] W.J.Boettinger, J.H.Perepezko, "Rapidly Solidified Alloys", ed. H.H.Liebermann, M.Dekker (New York), 1993, p.17

[9] L.Battezzati, P.Baldi, M.Baricco, E.Bosco, C.A.Goria, G.Serramoglia, F.Marongiu, Int. J. Cast Iron Met. Res. 16 (2003) 125

[10] P. Gustafson, Scan. J. Metall. vol 14, (1985) p 259-267

[11] Thermocalc A.B., SSOL database

[12] J.W.Elmer, S.M.Allen, T.W.Eagar, Metall. Trans. A 20A (1989) 2117

[13] E.Bosco, P.Rizzi, M.Baricco, Mat. Sci. Eng. A. 375-377 (2004) 468-472

[14] H. Okamoto, T.B. Massalski, L.J. Swartzendruber, P.A. Beck, in: H. Okamoto (Ed.), Phase Diagrams of Binary Iron Alloys, American Society for Metals, Metals Park, OH, 1993, p.33.

[15] L.Battezzati, M.Baricco, G.Riontino, I.Soletta, J. de Phys. 51 (1990) C4-79

[16] G.Cocco, I.Soletta, L.Battezzati, M.Baricco, S.Enzo, Phil. Mag. 61 (1990) 473

[17] N.Saunders, CALPHAD 9 (1987) 297

[18] H.Fenglai, N.Cowlam, G.E. Can, J.B.Suck, Phys. Chem. Liq. 16 (1986) 99

[19] L.Battezzati, Phil. Mag. B61 (1990) 511

[20] J.L.Murray, Metall. Trans. A 19 (1988) 243

[21] L. Battezzati, C. Antonione, M. Baricco, J. of Alloys and Compounds, 247 (1997) 164

[22] M. Palumbo, E. Bosco, G. Cacciamani, M. Baricco, CALPHAD, 25, 4 (2001) 625

[23] M. Palumbo, G. Cacciamani, E. Bosco, M. Baricco, Intermetallics 11 (2003) 1293

[24] U. Köster, U.Herold, Glassy Metals I, H.-J.Güntherodt and H.Beck eds., Springer-Verlag, Berlin (1981), p. 225

[25] T. Van Rompaey, K.C. Hari Kumar, P. Wollants, J. of Alloys and Compounds 334 (2002) 173-181

[26] C. Antonione, L. Battezzati, G. Cocco, F. Marino, Z. Metallkde 75 (1984), 714

[27] Q. Chen, B. Sundman, J. of Phase Equilibria 22 (2001) 63

[28] M. Baricco, L. Battezzati and P. Rizzi, J. Alloys and Compounds 220 (1995) 212

[29] O. Teppo and P. Taskinen, Mater. Sci. Tecn. 206 (1993) 211

[30] M.Baricco, F.Gaertner, G.Cacciamani, P.Rizzi, L.Battezzati, A.L.Greer, Mat. Sci. Forum 269-272 (1998) 553

[31] M.Baricco, M.Palumbo, J. Met. Nanoc. Mat. 20-21 (2004) 415-424

[32] A.Inoue, Prog. Mat. Sci. 43 (1998) 365

[33] M.Baricco, L.Battezzati, G.Borzone, G.Cacciamani, J. Chim. Phys. 90 (1993), 261

[34] I. Ansara, N. Dupin, H.L. Lukas, B. Sundman, J. All. Comp. 247 (1997) 20

[35] G. Cacciamani, R. Ferro, Calphad 25 (2001) 583

[36] M. Palumbo, G. Borzone, S. Delsante, N. Parodi, G. Cacciamani, R. Ferro, L. Battezzati, M. Baricco: Intermetallics 12 (2004) 1367-1372

ABSTRACT

FASI METASTABILI E DIAGRAMMI DI FASE

PAROLE CHIAVE: **metallurgia fisica, modellazione, trasformazione di fase, solidificazione**

La presenza di fasi metastabili è molto frequente nei materiali metallici e la loro formazione può essere descritta sulla base di considerazioni termodinamiche e cinetiche (figura 1). Uno stato metastabile si trova ad una energia maggiore rispetto al corrispondente stato di equlibrio e, sulla base della natura composizionale, strutturale o morfologica della metastabilità, può essere stimata la differenza di energia tra i due stati (tabella 1). Fasi metastabili possono essere prodotte mediante diverse tecniche, così come indicato in tabella 2.

Una volta nota l'energia libera di tutte le fasi in funzione della temperatura e della composizione, è possibile determinare il diagramma di fase d'equilibrio. Estrapolando l'energia libera della fasi stabili in ampi intervalli di temperatura e composizione e stimando l'energia libera delle nuove fasi metastabili, si può determinare anche un diagramma di fase metastabile. Questo è possibile minimizzando l'energia libera di Gibbs di tutte le fasi mediante l'approccio CALPHAD. Le informazioni termodinamiche sulle fasi metastabili risultano inoltre essenziali per la la modellizzazione della cinetica delle trasformazioni di fase. Con tale approccio è possibile descrivere il comportamento di sistemi che, per sottoraffreddamento della fase liquida, portano alla formazione di una fase amorfa. Questa situazione può essere rappresentata per mezzo delle curve T_0, che rappresentano il luogo dei punti in cui l'energia libera del liquido e di una fase solida della stessa composizione risultano uguali, così come mostrato in figura 3 per un sistema eutettico. Se, la fase liquida viene sottoraffreddata in condizioni di non equilibrio fino ad incontrare la curva T_0, risulta possibile una solidificazione senza ripartizione di soluto. Se le curve T_0 non si incotrano, riuslterà possibile individuare un intervallo di composizione per il quale il liquido può essere sottoraffreddato fino alla temperatura di transizione vetrosa, con conseguente formazione di una fase amorfa.

Diagrammi di fase di non-equilibrio trovano comune applicazione nella produzione di ghise e di acciai inossidabili. Nel corso di esperimenti di solidificazione rapida di leghe Fe-C è stata osservata una microstruttura che ha suggerito una solidificazione eutettica in condizioni metastabili, con formazione di ferrite e cementite. Al fine di giustificare tale comportamento, è stato effettuato un calcolo dei digrammi di stato Fe-C stabili e metastabili. I risultati sono mostrati in figura 3, dalla quale si può evincere che la solidificazione osservata può avvenire per un sottoraffreddamento del liquido di composizione eutettica di circa 50 gradi. I diversi modi di solidificazione degli acciai inossidabili possono essere descritti sulla base del digramma di fase ternario Fe-Ni-Cr, mostrato in figura 4 per una concentrazione di Cr pari al 18 % in peso. Agendo sulla velocità di raffreddamento è possibile selezionare il modo di solidificazione, per ottenere una miscela di fasi ed una microstruttura desiderata. Con tecniche di rapida solidificazione è inoltre possibile preparare soluzioni solide sovrassature, così come è stato fatto per il sistema Au-Fe. In seguito a trattamento termico, queste presentano l'interessante fenomeno della magnetoresistenza gigante, che si verfica ogni qualvolta nanoparticelle omogenee di materiale ferromagnetico sono inglobate in una matrice paramagnetica. In figura 5 sono mostrate le composizioni di alcune soluzioni solide, ottenute dall'analisi XRD di campioni riscaldati a varie temperature fino ad avvenuta precipitazione. Considerando le linee di solvus della fase FCC metastabile e della fase BCC stabile, ottenute col metodo CALPHAD, è stato possibile interpretare i processi di precipitazione osservati.

Considerando un contributo di eccesso al calore specifico della fase liquida, è stato possibile calcolare il diagramma metastabile per il sistema Cu-Ti, considerando che, per motivi cinetici, non sia possibile la formazione dei composti intermetallici. Il risultato è riportato in figura 6, mediante la quale è stato stimato l'intervallo di amorfizzazione limitato dalle curve T_0, che si è dimostrato vicino a quello determinato sperimentalmente. Nel sistema Al-Ti non è possibile ottenere fasi amorfe per rapida solidificazione, ma solamente per sintesi diretta di opportune miscele di elementi per mezzo dell'alligazione meccanica. Al fine di giustificare tale comportamento, sono state calcolate le curve T_0 per le soluzioni solide BCC, FCC e HCP. Il calcolo è stato effettuato partendo da dati di letteratura ed introducendo un calore specifico di eccesso per la fase liquida. I risultati sono confrontati in figura 7, dalla quale si evince che, per mezzo di un rapido raffreddamento, non può essere impedita una cristallizzazione del liquido nelle soluzioni solide senza ripartizione di soluto. Al contrario, per alligazione meccanica risulta possibile ottenere fasi amorfe.

Sempre con l'approccio CALPHAD è stato possibile effettuare un'analisi termodinamica del sistema Fe-B, per il quale è possibile formare una fase amorfe per composizioni vicino all'eutettico ricco in ferro. Sia mediante esperimenti di solidificazione che per cristallizzazione di leghe amorfe, si può formare il composto intermetallico metastabile Fe_3B. La figura 8 mostra sia il diagramma di fase d'equilibrio che il diagramma metastabile, ottenuto sospendendo il composto Fe_2B e rendendo così stabile la fase Fe_3B. Un ulteriore esempio di fase metastabile prodotta per effetto di un rapido raffreddamento è costituito dal composto $Ni_{23}B_6$. In figura 9 sono riportati i diagrammi di fase Ni-B stabile e metastabile, quest'ultimo calcolato sospendendo il composto Ni_3B e includendo la nuova fase $Ni_{23}B_6$. Tale fase metastabile si decompone, in riscaldamento, in Ni e in l'Ni_2B attraverso una reazione peritettoidica.

Anche per i sistemi Al-Ce e Al-Ce-Ni sono state effettuate ottimizzazioni termodinamiche delle fasi stabili e metastabili per studiare gli aspetti termodinamici e cinetici che promuovono la formazione di nanocristalli mediante cristallizzazione primaria di leghe amorfe. Il diagramma di fase Al-Ce d'equilibrio è mostrato in figura 10. Trascurando la formazione di composti intermetallici per motivi cinetici, è stato possibile calcolare il digramma di fase metastabile, dal quale risulta un ampio intervallo di composizioni in cui è possibile avere la formazione di fasi vetrose.

Per il calcolo del sistema ternario Al-Ce-Ni è stato necessario effettuare una ottimizzazione del sistema Ce-Ni, non disponibile in letteratura. In figura 11 è mostrata una sezione isoterma dei diagrammi di fase ternari stabile e metastabile. Il diagramma stabile prevede l'equilibrio tra le fasi solide fcc-Al, Al_3NI, e $Al_{11}Ce_3$, mentre in condizioni metastabili è stato considerato l'equilibrio tra le fasi liquido e fcc-Al. Dai valori della energia libera delle fasi solide e della fase liquida è stato così possibile calcolare la forza motrice per la nucleazione di Al in funzione della temperatura e della composizione, permettendo così una descrizione della formazione della fase nanocristallina.